Measurements of the static pressure near the surface in the atmospheric boundary layer

Measurements of the Static Pressure near the surface in the Atmospheric Boundary Layer

Roger Hoxey[1*], Peter Richards[2], Andrew Quinn[1], Adam Robertson[1] and Hannah Gough[3]

[1]School of Civil Engineering, University of Birmingham, B15 2TT, UK
[2]Department of Mechanical Engineering, University of Auckland, New Zealand.
[3]Department of Meteorology, University of Reading, Reading, RG6 6BB, UK.

(Received: DD Month YEAR/ Accepted: DD Month YEAR)

Measurements have been made of the three components of velocity and of the static pressure in the lowest 10 m of the atmospheric boundary layer. The measurements reported here were made on two occasions: the first with a single 10 m mast and the second with four 6 m masts. One-hour duration measurements at a sampling rate of 10 samples s^{-1} were processed for statistical properties including an assessment of the mean static pressure, and the time series processed for spectral properties. The mean velocity profile followed the expected boundary-layer log-region. An estimate of the mean static pressure compared to that above the boundary layer has been made and shows a dependency on the RMS (Root Mean Square) of dynamic pressure. The spectra of wind velocity and wind dynamic pressure follow the expected $n^{-5/3}$ power-law decay rate in the inertial subrange, whereas static pressure spectra followed a decay rate close to $n^{-4/3}$ - a result that was not predicted by published theory Limited comparisons have been made with measurements from wind-tunnel boundary-layer flows, and with one other full-scale experiment. There is evidence from these comparisons that the static pressure spectra has a decay rate close to $n^{-4/3}$ but there is also evidence of Reynolds-number sensitive. These measurements were made as part of a study of wind effects on buildings. The distinct spectral pattern of static pressure compared to that of dynamic pressure is a potential aid to identifying their separate contribution to wind loading and natural ventilation.

Keywords

Boundary layer flow, turbulence, static pressure, spectra.

*Corresponding author email: roger@hoxey.com

I. INTRODUCTION

Vorticity is inherent in all turbulent shear flows, including the atmospheric boundary layer (ABL), and evidence is now available (Hutchins et al. 2012) to show that fluid structures of large scales exist in the ABL. Rotational flow elements that, in boundary layers, are classified as coherent structures or eddies, range in size from millimetres to approaching the boundary-layer thickness, and in the case of atmospheric flows there are cyclonic flows including tornados and hurricanes that exist to a size of ~10^3 km. These flow structures have a distinctive static pressure pattern. The static pressure in a cyclonic weather system is familiar from forecast maps and is easily measured, but within the ABL the fluid structures contain a complex low-pressure core with smaller structures being embedded within larger ones; it is the static pressure variations in such flows that are the subject of this full-scale experimental study.

The term ‘static’ in Bernoullian flow refers to the contribution to total pressure excluding the dynamic pressure. In steady, irrotational flow, the total pressure is constant along a streamline and the static pressure is temporally constant but spatially variable. However, the unsteadiness associated with rotational elements within the flow results in the ‘static’ pressure being depressed and unsteady. Measurement of the static pressure within turbulent laboratory flows poses significant difficulty, particularly in thin boundary layers where a static probe is large in comparison to the boundary-layer thickness. Using a traditional pitot-static probe (Bryer & Pankherst 1971) also requires the probe to be aligned to the instantaneous flow as the static pressure sensed by the probe is sensitive to cross flow. Komerath et al. (1985) developed an alternative method of deriving fluctuating static pressure from the difference between total pressure, measured by a pitot probe, and the dynamic pressure, derived from a hotwire anemometer. The pitot probe is relatively insensitive to misalignment to the instantaneous flow direction in comparison to the static pressure from a pitot-static probe.

Measurements made in laboratory boundary-layer flows are often restricted to sensing velocity and occasionally the pressure at the surface (Goody 2004). An exception to this is the work of Tsuji et al. (2007) who used a small static probe: this study measured the static pressure through the boundary layer and also at the surface. Their work included mean static pressure profiles and spectral patterns. They also reviewed earlier work on the measurement of static pressure with an emphasis on spectral properties and comparisons with theoretical expectations.

61 The proposal based on Kolmogorov (1941) and often referred to as Kolmogorov's power-law of a
62 -7/3 logarithmic decay failed to explain the limited measurements reviewed in Tsuji et al. (2007)
63 and also failed to fit their more detailed measurements. Both Goody (2004) and Tsuji et al. (2007)
64 showed that static pressure spectra are sensitive to Reynolds number and there is experimental
65 evidence of Reynolds-number sensitivity in vortices associated with recirculating flows around
66 bluff bodies (Lim et al. 2007). This has been observed in both the stable and intermittent vortices
67 generated by a bluff body (Hoxey et al 1998). The evidence of Reynolds-number sensitivity in
68 vortex flows associated with bluff bodies raises questions about similar sensitivity with vortex
69 elements in turbulent boundary-layer flows.
70 Computational methods are being developed to model the ABL. Miles et al. (2004) used
71 large-eddy simulation (LES) to model three ABLs with free convection, forced convection, and
72 stable stratification. Their spectral results for static pressure in the stable boundary layer cast
73 further doubt on the -7/3 decay as their computed spectra have a higher value in the inertial
74 subrange, which from their presentation appears close to -4/3. They also point out that to resolve
75 computational uncertainty "it is probably necessary to measure the pressure spectrum in high
76 Reynolds-number flows to settle this issue".
77 The ABL is of sufficient size to enable a more detailed study of static pressure fluctuations
78 to be made at higher Reynolds number and also at generally higher turbulence levels. The ABL
79 can also accommodate sensors which produce little disturbance to the flow. In the experiments
80 described in this paper, the temporal static pressure to a height of 10 m has been measured using
81 'static' pressure probes (Moran and Hoxey 1979).
82 Two sets of measurements are described in this paper, the first made in 2000 of the vertical
83 profile of velocity and static pressure, and the second made in 2015/16 of both the vertical and
84 horizontal variation in static pressure. The reason for this latter experiment was to explore the
85 spatial variation of static pressure and also to assess the contribution to ventilation driven by static
86 pressure fluctuations on a naturally-ventilated building.
87 Comparisons are made with static pressure measured in the ABL by Albertson et al. (1998),
88 and comparisons are presented with surface pressure fluctuations in boundary-layer flows at
89 relatively low Reynolds number reported by Goody (2004) and Tsuji et al. (2007).
90 Where appropriate, the statistical properties of wind dynamic pressure and of static pressure,
91 including an estimate of mean static pressure, are presented for information, including an

assessment of the mean static pressure in the boundary layer based on turbulence intensity, but the primary objective is to detail the spectral properties of static pressure. Since the findings of this did not comply with theoretical prediction, and since an alternative theoretical method was not forthcoming, a simplified vortex model of Eulerian flow, described in Appendix B, was explored to assist in the understanding of the experimental findings.

2. MEASUREMENTS OF STATIC PRESSURE IN THE ABL

Two sets of measurements have been made of the static pressure within the ABL on the experimental site at Silsoe, UK. For the measurement of static pressure, static probes were used for above-ground measurements, and at the ground a conventional ground-level tapping hole was used. The probes are insensitive to horizontal flow direction and only slightly sensitive to the vertical component of flow. Wind velocity was measured by 3-component sonic anemometers.

.

2.1. Site details and instrumentation

The site at Silsoe (52.00852ºN, 0.42378ºW) is flat and well exposed to the west for 400 m; to the south there are buildings 250 m away. The immediate surrounding area was cut grass and beyond this the land was cultivated with low level crops or maize stubble at the time measurements were made. The site has been used for many years for the measurement of wind load on buildings which were constructed for that purpose (for example Richards et al 2001). More recently the site has been used for the study of natural ventilation using the 6 m cube (Gough et al 2018). Velocity profile measurements (Hoxey & Richards 1992) show a good fit to a log-law with a typical surface roughness parameter z_o of 10 mm for winds from the SW to NW; higher z_o values were measured for winds from S to SW, as found in the 10 m mast measurements reported below.

For the measurement of static pressure, static probes (Moran and Hoxey 1979 and reviewed in Appendix A) were used for above-ground measurements. These cylindrical, axis-symmetric probes (165 mm in height by 28 mm in head diameter) are mounted vertically and consequently their performance is insensitive to horizontal flow direction; they are also suitable for use in rain. The design of the probe is a scaled-down version of a static probe for use in atmospheric flows first proposed by Marshall (1976). Alternative designs of static probe have been developed for turbulent flow, for example Nishiyama and Bedard (1991) who also include the probe used here in their review.

123 The probes developed at Silsoe Research Institute were first used on full-scale buildings to
124 replace surface roof tappings which were susceptible to being blocked. The probes were initially
125 calibrated by mounting them at a height of 3 m above a ground tap on an exposed, cut-grass site.
126 This full-scale calibration procedure was followed by wind-tunnel comparisons in low-turbulence
127 flow, and a consistent pressure coefficient difference of +0.07 was observed. For the measurements
128 of static pressure in the ABL, the probes were calibrated in a low-turbulence wind tunnel and set
129 to agree with the static pressure at a wall tap at the probe position in the working section of the
130 wind-tunnel in the conventional manner for calibrating static probes. It was apparent from the
131 consistent difference between these two calibration methods that the probes were sensitive to the
132 static pressure field associated with turbulent flow in the ABL, and that by implication it is the
133 eddies in turbulent flow that were responsible. At this time (in the 1980's), the authors were not
134 aware of any other measurements in the ABL. It was not until Albertson et al published their
135 findings in 1998, using a different probe based on two horizontal flat plates, that these observations
136 were corroborated. Details of the probe design used in the current study, and its sensitivity to air
137 speed and pitch are described in Appendix A. All the probes used in these experiments were
138 individually calibrated in a low-turbulent wind-tunnel flow within an overall estimate of error of
139 ±1½% of wind dynamic pressure.
140 The probes have a sensing head of 28 mm in diameter, giving a potential response to eddies
141 of this size and larger. Static pressure was also sensed at the ground with a conventional ground-
142 level tapping hole of 9 mm diameter with a potential response to eddies of this size. In the
143 experiments described here, it is the 6 mm internal diameter tubing connecting the sensors to the
144 transducers that limits frequency response. The shortest tube lengths used were 1 m, giving a flat
145 response to ~70 Hz, and the longest tube of 15 m gives a flat response to ~5 Hz. Individual
146 differential pressure transducers (Honeywell Differential Pressure Sensor 163PC01075 ±2½
147 inches of H_2O, ± 635 Pa) were used for each sensor. The pressure transducers have a flat response
148 to over 50 Hz but again this is limited by the tubing. The conversion from analogue to digital gave
149 a pressure resolution of 0.026 Pa/count.

150 The backing pressure for all the measurements was from a ground tapping which consisted
151 of a 100 mm aluminum can buried in the ground flush to the surface with a 9 mm tapping hole.
152 The pressure from this tapping was conveyed by 6 mm internal diameter tube and was
153 pneumatically averaged using a restrictor/volume combination with a response of ~100 s. This

backing pressure was connected to each of the pressure transducers via a manifold. There are practical difficulties in finding a suitable backing pressure as small changes in temperature and atmospheric pressure will affect the air in the volume (a large earthenware bottle) which will become apparent in the low frequency part of the static pressure spectrum. Low frequency fluctuations in pressure occur in windy conditions and cannot be eliminated, but for the measurements reported here there were near constant temperature conditions which minimize this effect.

Symmetrical head three-component ultrasonic anemometers (3-D Wind Master Sonic Anemometer manufactured by Gill Instruments) were used to measure the three components of air velocity and also the speed of sound: as the speed of sound relates to air temperature, the instrument was used to calculate heat flux. The anemometer has a path length of 150 mm which attenuates response to eddies smaller than two to three times this path length. The anemometer was used as the timing device for the data recording, in this case set to 10 samples s^{-1}. The frequency response will depend on air velocity; for flows below 3 m s^{-1} (20 x path length), response to 10 Hz with attenuation can be expected. In the measurements reported here, streamwise wind speed was above 5 ms^{-1} with no significant attenuation in the measurements, although the opposite effect on spectra of aliasing is likely to affect the frequencies below the Nyquist frequency.

The spectral analysis of the static pressure measurements is restricted to curve fitting over that part of the inertial subrange for which measurements were made. To identify the extent of the inertial subrange (defined as the frequency range where the spectrum of velocity has a logarithmic decay of -5/3) the spectra of the three components of velocity (u', v' and w') are shown in figure 1. This is for an average of two non-overlapping records of 4096 data points at 10 samples s^{-1}. This figure confirms an inertial subrange from approximately 0.005 Hz to 5 Hz and it may extend to both lower and higher frequencies, but record length and instrumentation response were insufficient to establish this. Logarithmic curve fitting over the full range will be used for all analysis in this paper. Unpublished measurements with hot wire anemometers mounted at a height of 1 m beside a sonic anemometer on the Silsoe site have shown that the inertial subrange extends well beyond 50 Hz, but the sonic anemometer measurements are not reliable above the Nyquist frequency of 5 Hz. The energy spectrum of wind dynamic pressure has the same logarithmic spectral decay of -5/3 as that of velocity, since velocity has to be squared (and multiplied by air density) to give an energy spectrum. The wind dynamic pressure spectrum is used in the analysis

that follows for comparison with static pressure spectra as they are dimensionally consistent. This requires that pressure energy spectra are computed by Fast Fourier Transform (FFT) and not via the autocorrelation method, as this effectively squares the input quantity.

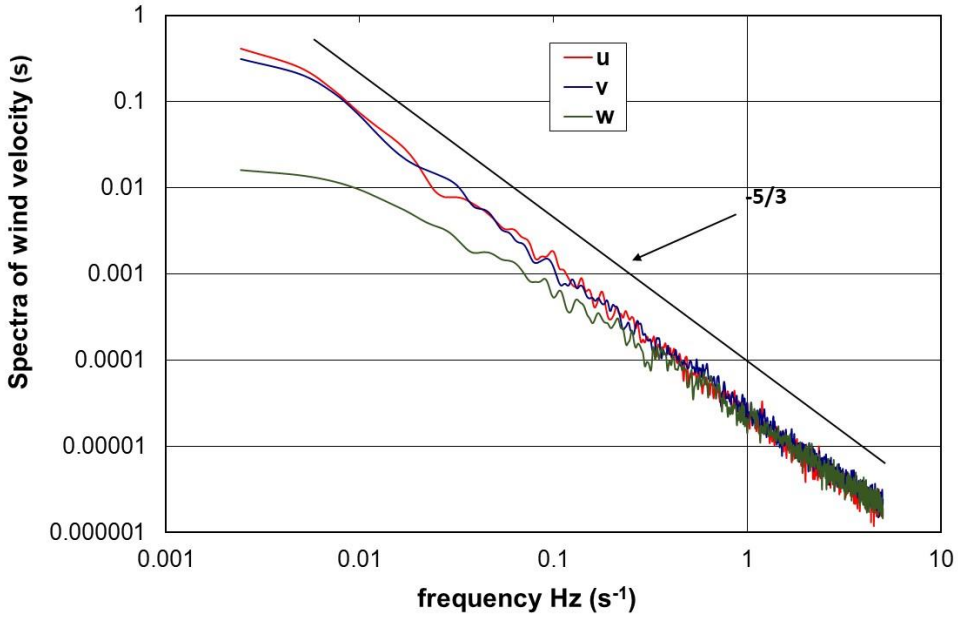

FIGURE 1 Spectra of the 3-components of velocity measured at a height of 6 m. The spectral density for all the components have been divided by the integrated spectrum of the streamwise component.

2.2. Single 10-m Mast

The first measurements, in March 2000, were of the static pressure on the site at Silsoe, at 1, 3, 6 and 10 m above ground. The static probes were mounted vertically on brackets horizontally off-set by 1 m from a 10m mast. The pressures from the static probes were measured against a backing pressure from the pneumatically-averaged pressure (time constant ≈100 s) from a tapping hole in the ground. Three-component sonic anemometers were also mounted at 1, 3, 6 and 10 m above ground on the same mast, but horizontally off-set to avoid interference with the static probes and the mast. Synchronised measurements of static pressure and of wind velocity from the sonic anemometers were collected at 10 samples s^{-1} for 60-min records (36,000 data points) and processed as four 15-min records. Four pressure transducers were positioned on the mast each with a 1 m length of 6 mm diameter tube connected to a static probe.

The one-hour of measurements reported here were made on the 29th March 2000 commencing at 09.58 GMT (sun rise 05.48 GMT). The measured heat flux, derived from the sonic

anemometers, and z/L where L is the Obukhov length, are given in table 1. These values of z/L are indicative of near-neutral atmospheric stability.

z (m)	$\overline{w'\theta'}$ (ms^{-1}K)	z/L
1	-0.0029	0.0002
3	-0.0005	0.0001
6	0.0035	-0.0016
10	0.0279	-0.0202

TABLE 1. Heat flux and atmospheric stability measured at the four heights

The streamwise mean-velocity profile, derived from the sonic anemometers, is shown in figure 2. This is well represented by a log-law of the form $U_z = \frac{u_*}{\kappa}\ln(z) + constant$, where U_z is the velocity at height z, u_* is the frictional velocity and κ is the von Karman constant. Defining a roughness length z_o where $U_{zo} = 0$ gives $U_z = \frac{u_*}{\kappa}\ln(\frac{z}{z_0})$. Extrapolating from a least-squares curve fit gives z_o = 90 mm and hence $u_{*/K}$ = 1.39 m s^{-1} ($u_* = 0.57$ m s^{-1} with $\kappa = 0.41$). The mean velocity (U_z), turbulence intensities (I_u = RMS(u)/U, I_v = RMS(v)/U and I_z = RMS(w)/U) and a velocity u_τ from the local Reynolds stress ($u_\tau = (-\overline{u'w'})^{1/2}$) derived from the sonic anemometers for the average of the four records, are given in table 2.

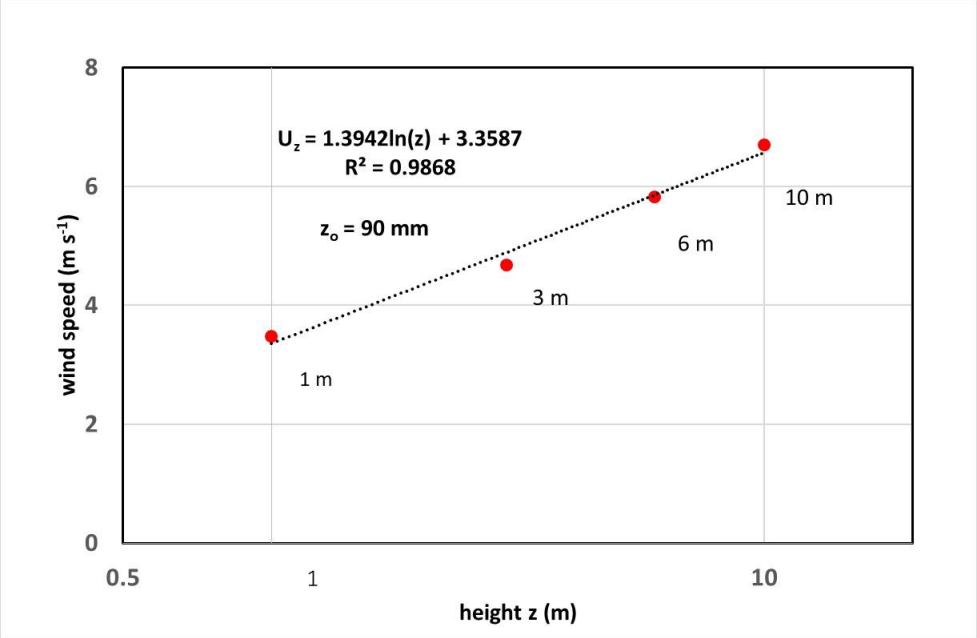

FIGURE 2. One-hour mean velocity profile with least squares estimate of U_z and z_o.

z (m)	U_z (m s^{-1})	I_u	I_v	I_w	u_τ (m s^{-1})	$\frac{u_\tau}{U_z}$
1	3.48	0.44	0.40	0.23	0.25	0.071
3	4.68	0.34	0.27	0.21	0.50	0.107
6	5.82	0.30	0.24	0.16	0.65	0.112
10	6.70	0.28	0.22	0.13	0.71	0.106

TABLE 2. Velocity-profile statistics (mean streamwise velocity (U_z), turbulence intensities (I) and a velocity from the local Reynolds stress (u_τ)) derived from the four sonic anemometers: average of four 15-min records.

The turbulence intensities are high compared with previous measurements on the site (I_u 0.18, I_v 0.15, I_w 0.08 at z = 6 m, Richards et al., 2000) and relate to the high roughness length (z_o) which occurs for winds on this site from the south. The statistics are from 15-min records and the inherent non-stationarity of the flow means that the standard deviation of the velocity components are sensitive to, and increase with, record length. The frictional velocity u_τ derived from the product of u' and w' is not reliable at low height as there is insufficient frequency response from the 10 Hz sonic anemometer. At a height of 1 m, a significant proportion of the stress may not be measured (Richards et al., 2000). The assessment of frictional velocity (u_τ) from the sonic

anemometers (table 2) is thus considered to be reasonably consistent with the assessment of frictional velocity of $u_* = 0.57$ m s^{-1} obtained from the velocity profile.

An example of the dynamic pressure, derived from the three-component sonic anemometer, and of the 'static' pressure measured at a height of 6 m in the ABL is shown in figure 3. (Note: 'true' zero for static pressure is not known; the static pressure data shown are with reference to a long-term static pressure average at ground level). There is interaction between the two quantities as both respond to eddies in the shear flow but there is a complex correlation as the dynamic pressure can be above or below that of the mean flow, whereas the static pressure is mainly negative. The 'spikes' in the record are associated with an eddy vortex centre passing very close to the sensor at the time of sampling. With a mean flow of 5 m s^{-1}, the static pressure is being sampled every 0.5 m of the flow, and with many eddies smaller than this the core pressure is often missed.

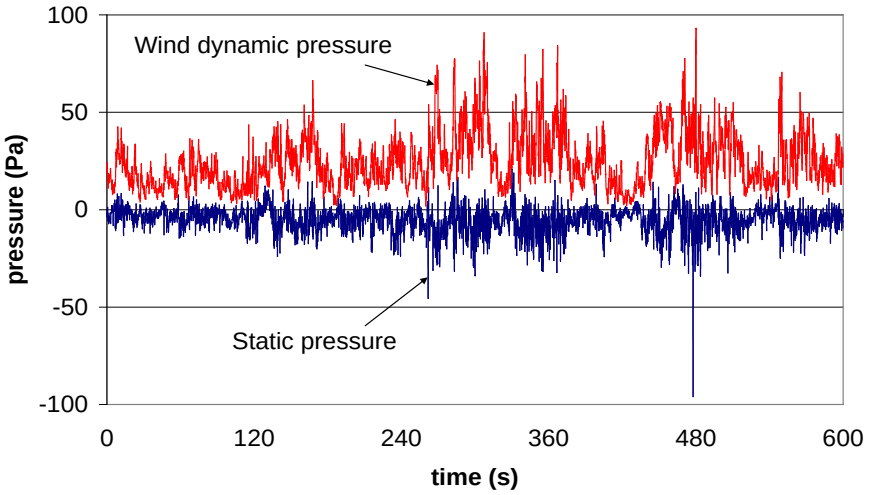

FIGURE 3. Example of the wind dynamic and static pressure in the ABL at a height of 6 m.

Energy spectra of wind dynamic pressure ($E_q(f)$) static pressure ($E_p(f)$) and of the Reynolds stress cospectrum ($-\rho u'w'$), all measured at a height of 6 m, are shown in figure 4. The spectra are non-overlapping averages of eight data sets of 4096 points with smoothing applied to the spectra before averaging. All the spectra shown are divided by the integrated spectrum of wind dynamic pressure and therefore magnitudes are comparable.

The wind dynamic pressure energy spectrum has the familiar characteristic of a -5/3 logarithmic decay rate, whereas the static pressure spectrum shows a reduced decay rate

approximating -4/3; a result that was not expected. The Reynolds-stress cospectrum does not exhibit a linear power-law decay, but has a decreasing value (more negative) from around -4/3 through -5/3 to -2 as frequency increases. The theoretical value of -7/3 may well be reached at higher frequency but there is insufficient sampling rate and resolution here to confirm this. There is also little contribution to the overall stress from higher frequencies (Hoxey & Richards 1992, Hoxey & Richards 1995, Richards et al 1997).

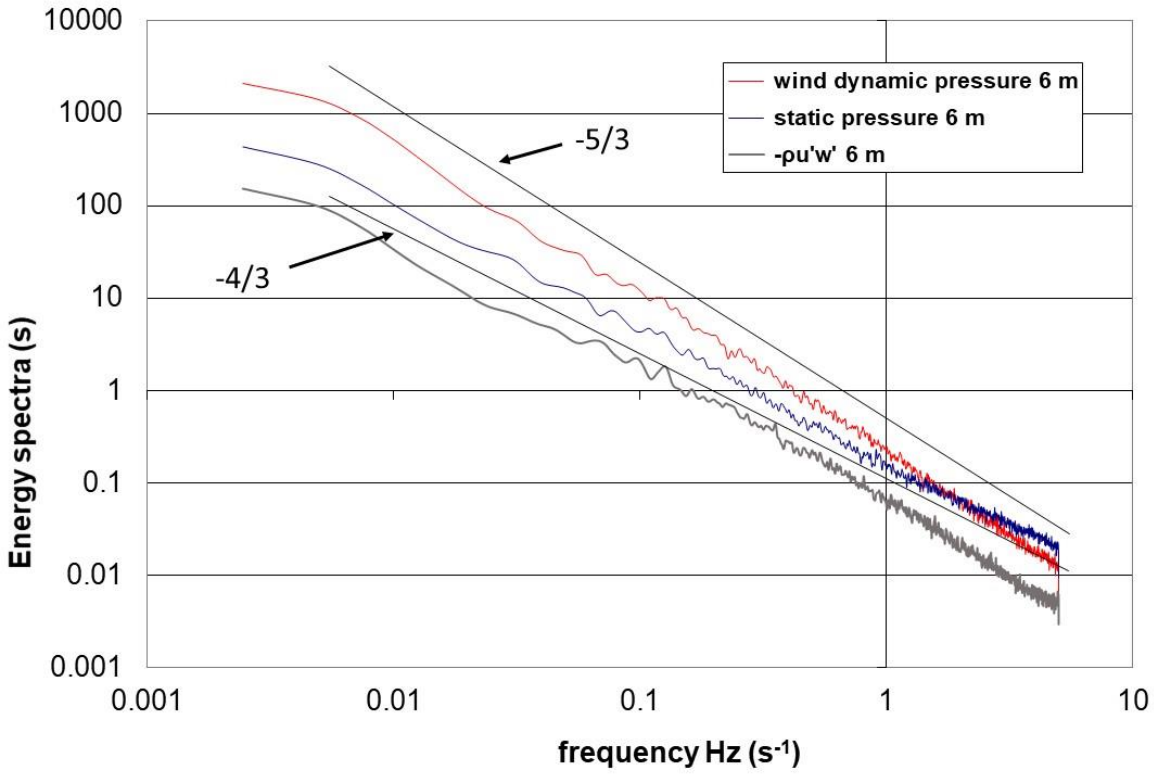

FIGURE 4. Energy spectra of wind dynamic pressure and static pressure, and also of the Reynolds-stress cospectrum, ($-\rho u'w'$), measured at a height of 6 m. All spectra divided by the integrated spectrum of the wind dynamic pressure

The exponents of frequency obtained by a least-squares curve fit for both wind dynamic pressure and static pressure spectra are given in table 3. The mean and standard deviation values are for eight non-overlapping periods of 409.6 s. The curve fit was over the frequency range 0.00244 to 5 Hz (2048 data points) and was not sensitive to the spectral smoothing method used. The pressure instrumentation is fully responsive over this range and no filtering was applied. The dynamic pressure spectrum shows a slight increase in the exponent with reduced height as the inertial subrange region moves to higher frequency. This is discussed in Richards et al. (2000).

z (m)	Exponent for wind dynamic pressure spectra (standard deviation)	Exponent for static pressure spectra (standard deviation)
1	-1.69 (0.030)	-1.39 (0.033)
3	-1.68 (0.026)	-1.36 (0.020)
6	-1.75 (0.014)	-1.36 (0.020)
10	-1.77 (0.006)	-1.32 (0.043)

TABLE 3. Exponent of frequency for wind dynamic pressure and static pressure for the 10 m mast measurements.

2.3 Four 6-m Masts

The second set of measurements was made in December 2015 / January 2016. The objective was to measure the static pressure at 1, 3 and 6 m on 4 masts positioned on the four side faces of an imaginary 6-m cube: the pressures were also measured at ground level, 0.5 m upstream of each mast base in vertical alignment with the probes, using hole-in-the-ground tappings. The experimental arrangement is shown in f5. The backing pressure for all the probes and ground taps was from another ground tap with a low-pass pneumatic filter (time constant ≈100 s). For reference, a 3-component sonic anemometer was mounted on a separate mast to the side of the array, and can be seen in figure 5.

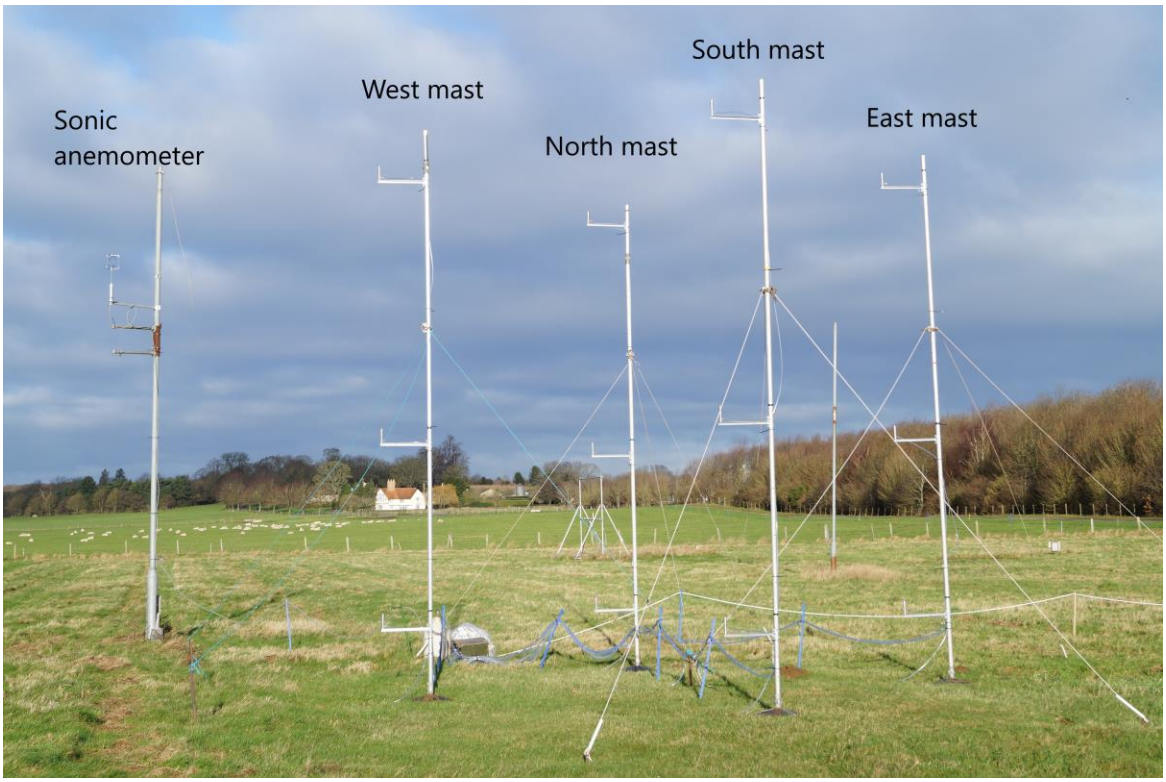

FIGURE 5. The four masts with static probes mounted to the windward side of the masts (flow from left to right): the reference sonic anemometer is on the windward-most mast. The flow was from west-south-west and the alignment of the east to west masts was 240° magnetic

Synchronised measurements of static pressure and of wind velocity from the sonic anemometer were collected at 10 samples s^{-1} for three 20-min records (36,000 data points). The one hour of records reported here were made on the 24th December 2015, commencing at 04.45 GMT (sun rise 08.10 GMT). The measured heat flux, derived from the 6 m sonic anemometer, was -0.0076 m s^{-1} K and z/L = 0.0041; indicative of near-neutral atmospheric stability. Measured statistics of the boundary layer based on the sonic anemometer at 6 m are given in table 4.

z (m)	U_z (m s^{-1})	I_u	I_v	I_w	u_τ (m s^{-1})	$\frac{u_\tau}{U_z}$
6	8.61	0.188	0.169	0.082	0.577	0.067

TABLE 4. Velocity profile statistics derived from the average of the three 20-min records from the sonic anemometers.

Compared with the measurements made in 2000, the turbulence intensities are lower and consistent with winter measurements on the site for a WSW wind, with a roughness length (z_o) of approximately 10 mm (Richards et al. 2000). The ratio u_τ/U_z is correspondingly lower.

The spectral properties, derived from six non-overlapping 409.6 s records of the wind dynamic pressure, and of the static pressure at the ground and at 1, 3 and 6 m are shown in figure 6. As with the single-mast measurements, the spectra of wind dynamic pressure and of static pressure follow closely a power-law decay. There is little observable difference for the above-ground static pressure spectra (all non-dimensionalised by the integrated spectrum of the wind dynamic pressure at 6 m), but the ground static pressure shows low frequency attenuation as a result of using a time-averaged differential backing pressure which included correlated low-frequency fluctuations. The mean value and standard deviation of the derived exponents for six non-overlapping periods are given in table 5: the wind dynamic pressure is the average of 6 data sets, whereas the static pressure is the average for the four masts, each of 6 data sets.

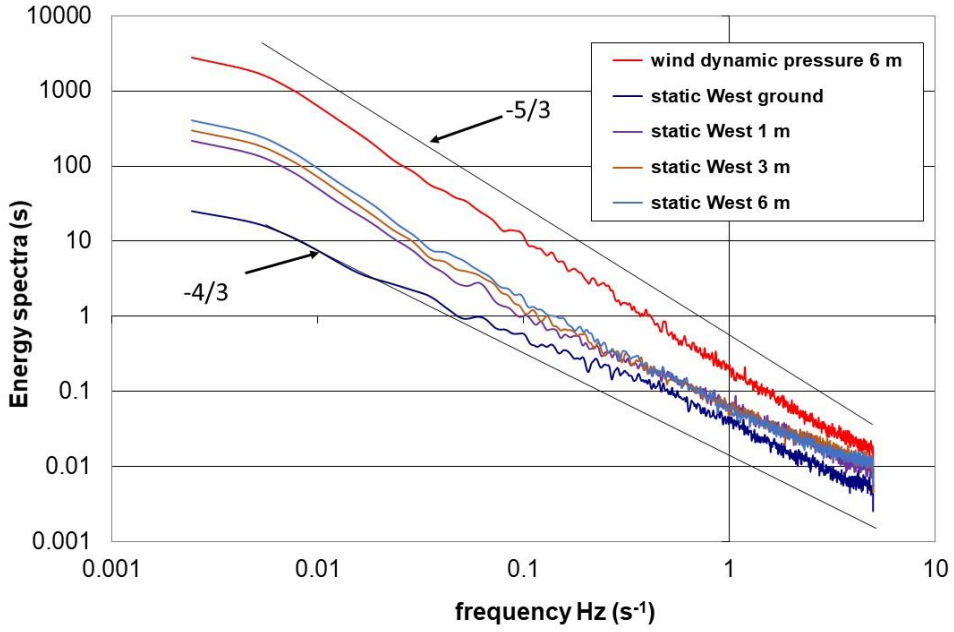

FIGURE 6. Energy spectra of wind dynamic pressure, static pressure at the ground and at 1, 3 and 6 m, derived from six non-overlapping 409.6 s records. All spectra divided by the integrated spectrum of the wind dynamic pressure.

z (m)	Exponent for wind dynamic pressure spectra (standard deviation)	Exponent for static pressure spectra (standard deviation)
ground		-1.28 (0.056)
1		-1.27 (0.035)
3		-1.33 (0.032)
6	-1.66 (0.002)	-1.38 (0.033)

TABLE 5. Exponent of frequency for wind dynamic pressure and static pressure.

The Reynolds-stress cospectrum shown in figure 7 followed the same pattern as noted above (figure 4) for the measurements made in 2000.

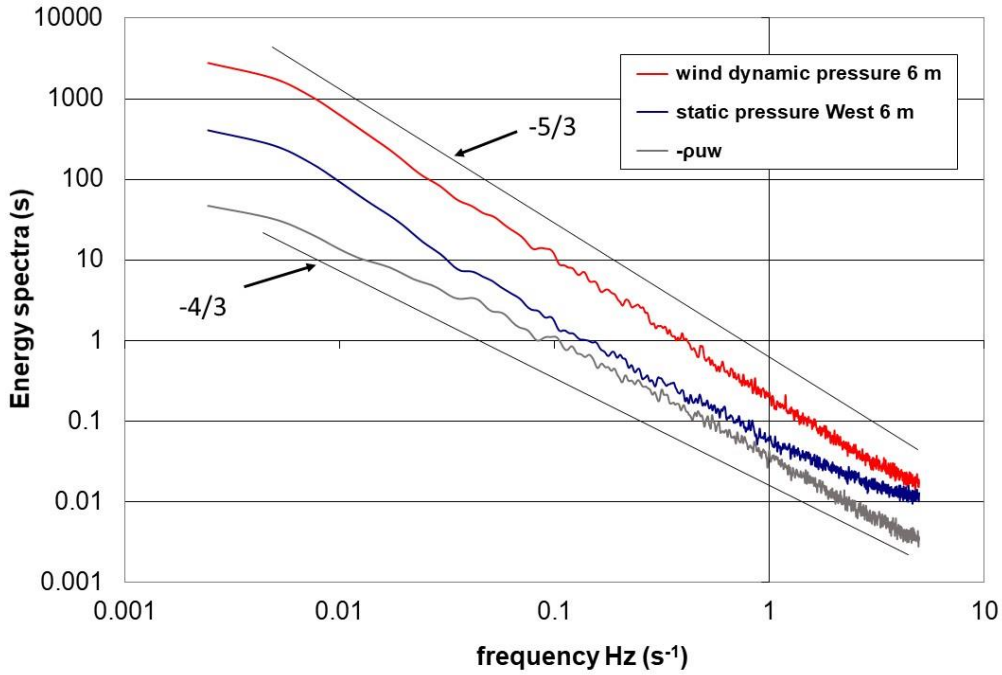

FIGURE 7. Energy spectra of wind dynamic pressure and static pressure, and also of the Reynolds-stress cospectrum, ($-\rho u'w'$), measured at a height of 6 m. All spectra are divided by the integrated spectrum of the wind dynamic pressure

The pressure transducers were positioned on the ground to the north of the North mast and tube lengths to the 6-m high static probes were up to 15 m. These tubes have a resonant frequency as low as 5 Hz which may contribute to the slight increase in the spectrum at this frequency: the

lower probes and ground taps with shorter tubes are not likely to be affected by tube resonance. The mean of the exponent for the static pressure measurements, including the ground taps, is -1.313 ($\frac{\sigma}{\sqrt{n}}$ = 0.009).

The cross-spectral density function has been calculated for the West and East static pressure at 6 m (aligned with mean flow direction) and also for the North and South static pressures (perpendicular to flow direction). The derived coherence function (Otnes and Enochson 1972) for each is shown in figure 8.

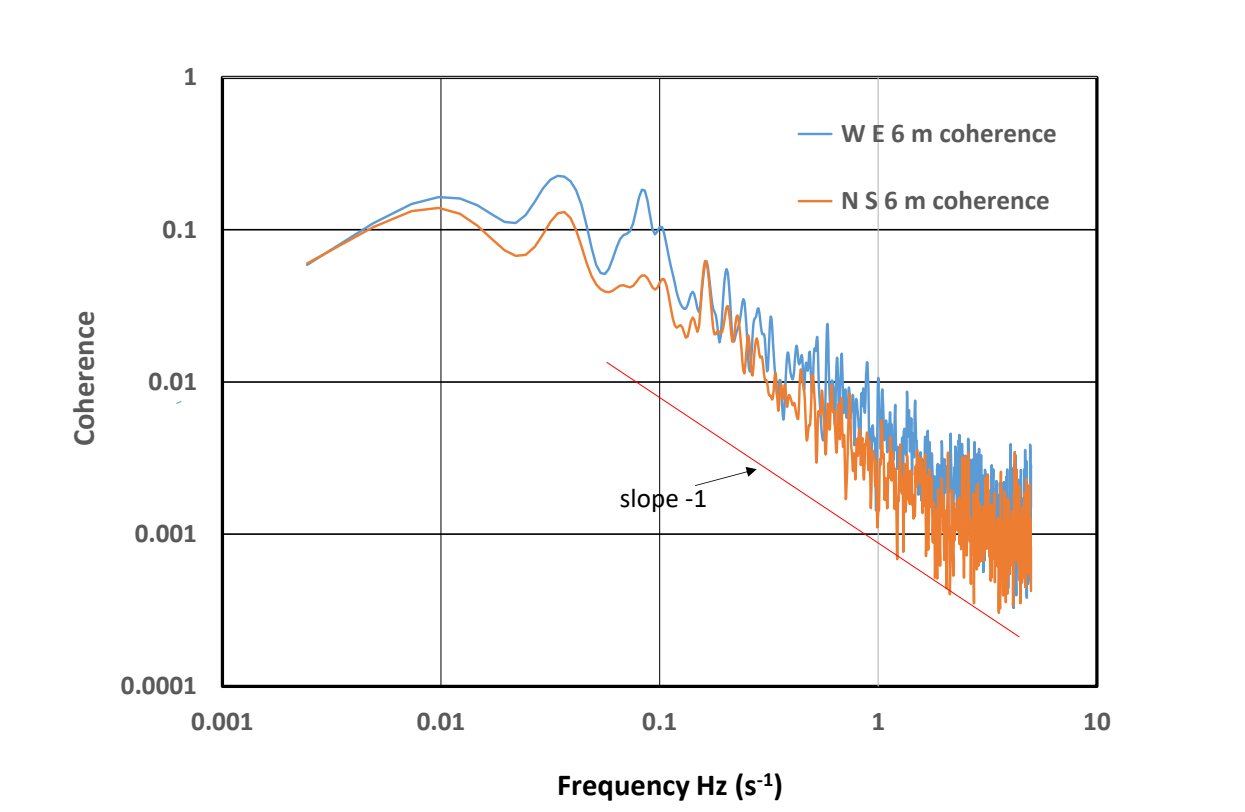

FIGURE 8. Coherence function of static pressure for aligned flow (West to East masts) and cross flow (North to South masts)

The coherence (figure 8) is greater for the aligned flow as expected but it also shows that the static pressure is spatially variable even for larger eddies as it is the small cores of these eddies that make the most significant contribution to static pressure. There is a clear need for a longer record in order to approach unity at low frequency.

3. MEAN VALUE OF STATIC PRESSURE

The measurements described here of static pressure are made with reference to the average surface pressure at the ground. Assessment of the 'true zero' mean static pressure within the boundary layer is speculative as it is impractical to relate it to the static pressure in the free-stream above the boundary layer (ABL thickness δ ~1 km). The complex structure of the turbulent boundary-layer flow, described for example by Morrison et al. (1992) and Hunt and Morrison (2000), with terms such as 'sweeps' and 'splats', leads to uncertainty about the transient positive static pressure that can occur within the flow. It appears (figure 3) that the influence of vortical structures (sweeps) dominate with negative static pressure, whereas 'splats' with positive pressure appear small in comparison. In a thin boundary layer, Tsuji et al. (2007) noted that 'the wall pressure is slightly lower than the free-stream pressure', an observation consistent with near-wall eddies depressing the wall pressure.

The probability density function (PDF) for static pressure measured on the West 6-m mast and at the ground are presented in figure 9. The statistics are given in table 6 for a 20-min record of 12000 data points. In all cases the static pressure is measured with reference to the time averaged pressure at the ground.

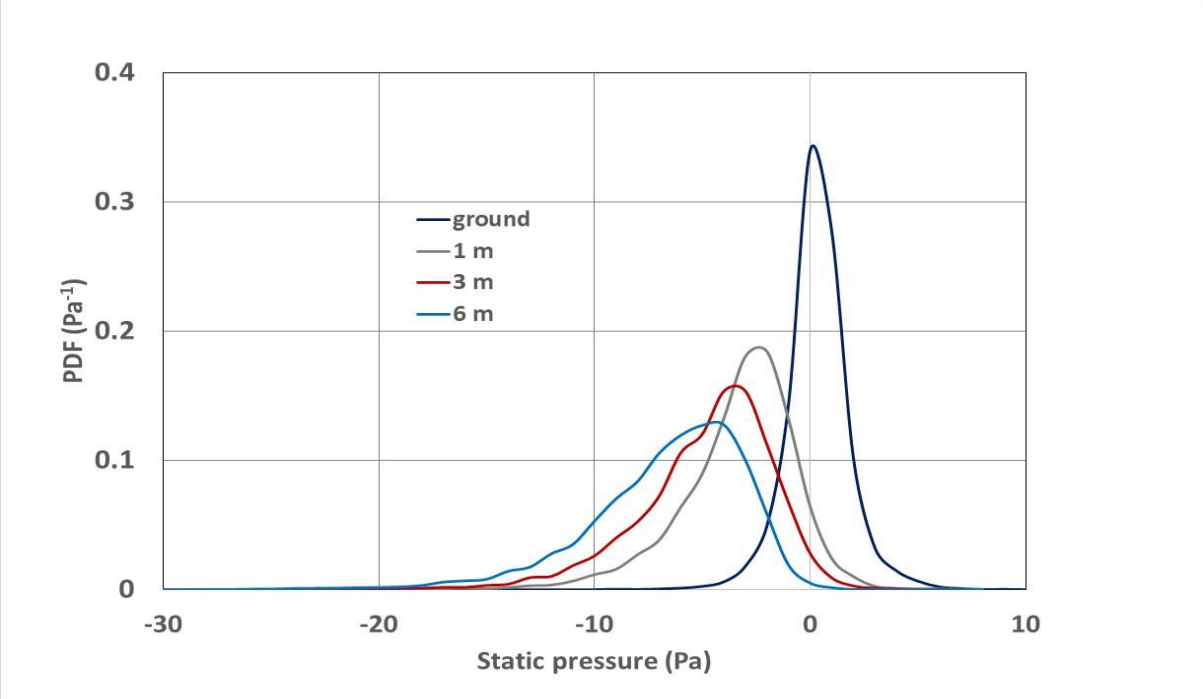

FIGURE 9. Probability density functions for static pressure measured on the West mast and at the ground.

z m	ground	1 m	3 m	6 m
Minimum (Pa)	-9.8	-29.5	-27.1	-28.3
Maximum (Pa)	10.6	11.7	5.8	6.3
Mean (Pa)	-0.16	-3.84	-5.33	-7.12
Standard deviation (Pa)	1.46	2.78	3.17	3.64
Skewness	0.001	-1.19	-1.07	-1.19
Kurtosis	6.81	7.18	5.40	5.47

TABLE 6. Statistics of the static pressure measured on the West mast and at the ground.

The PDF of ground static pressure is distinct from above ground measurements as eddies can only pass near the ground, but above ground they can pass through the probes. The core pressure in eddies skew the PDF of the probe measurements and give a lower mean pressure. The measured mean dynamic pressure ($q_{mean\,z}$), the mean pressure difference ($p_z - p_0$), and RMS values of dynamic and static pressure are presented in tables 7 and 8, with an additional column, Cp_z, defined as $Cp_z = (q_{RMS}^2 - p_{RMS}^2)^{1/2}/q_{mean\,6}$. Numerically Cp_z is the displacement value to align q_{rms} with the square root of the second moment of p.

z m	q_{mean} (Pa)	$q_{RMS}/q_{mean\,z}$	p_z-p_o (Pa)	$p_{RMS}/q_{mean\,z}$	Cp_z
0			zero	N/A	-0.195*
1	10.44	0.734	-2.36	0.435	-0.254
3	16.61	0.617	-4.10	0.335	-0.356
6	24.30	0.553	-5.09	0.245	-0.496
10	31.38	0.507	-4.93	0.201	-0.601

TABLE 7. Mean static pressure analysis for the 10- m mast measurements (* denotes value derived from curve fit)

z m	q_{mean} (Pa)	q_{RMS}/q_{mean}	p_z-p_o (Pa)	$p_{RMS}/q_{mean\ 6m}$	Cp_z
0			zero	0.029	-0.143*
1			-3.80	0.055	-0.185*
3			-5.53	0.062	-0.260*
6	46.02	0.369	-6.61	0.069	-0.362

TABLE 8. Mean static pressure analysis for the four 6-m mast measurements. (* denotes values derived from curve fit)

The values of Cp_z are shown in Fig 10 and the curve fit extrapolated to the ground (z = 0) giving a static pressure coefficient at the ground Cp_0. As the PDF of the ground tap is close to a symmetric distribution, Cp_0 corresponds to the maximum value of the static pressure, and Cp_0 can be considered as the static pressure at the ground. The proposed explanation for this is that the fluctuations of dynamic pressure are centered on the mean as the vortices can pass either side of the measurement point and can rotate in either direction. Whereas the fluctuations in static pressure associated with all eddies are negative compared to the mean static pressure. Hence for comparison with q_{RMS}/q_{mean} the static pressure fluctuations must be calculated as the square root of the mean of the second moment about an offset pressure. This offset is the proposed 'true zero' static pressure at the ground.

This 'true zero' static pressure can be considered as the static pressure in the absence of turbulence effects in the flow above the boundary layer. In the skewed PDF of static pressure above ground the same approach cannot be adopted. This is confirmed in Fig 10 where the measured pressure difference $(p_z - p_0)/q_{mean\ 6m}$ has been added to Cp_0 giving data points above Cp_z for z > 3 m. The relationship between turbulence and static pressure fluctuations was also commented on by Tsuji et al (2007) who concluded that 'The ratio $p_{rms}/\rho u^2_{rms}$ was found to be of the order of one'.

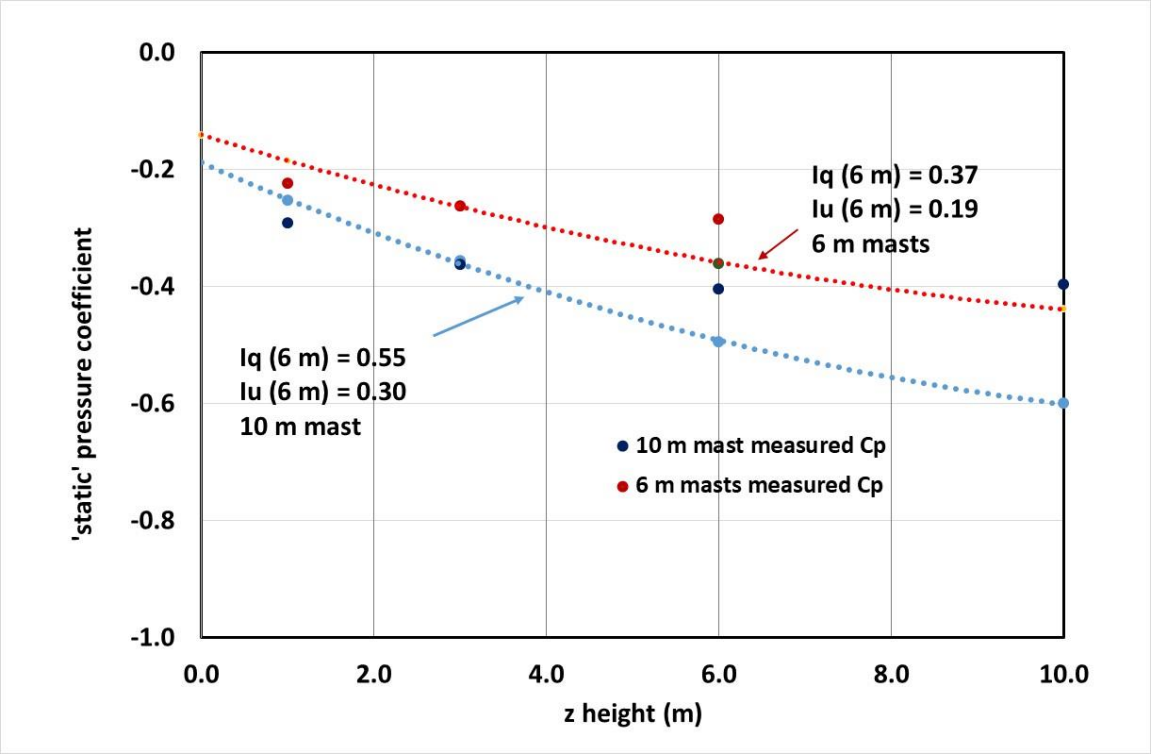

FIGURE 10. Calculated static pressure coefficients: 10 m mast values in blue (4 points) and 6 m mast value in red (3 points). The dashed lines are curve fits to Cp_z extrapolated to z = 0 to give Cp_0.

The values given in Table 8 for the mean static pressure at the ground (Cp_0 = -0.143) gives an off-set to the pressures in the PDF in figure 9 of -6.54 Pa. Applying this off-set gives a probability level of ≈ 0.1% of the measured static pressure at the ground being greater than zero, suggesting that there are only a few intermittent positive static pressures values above the 'true zero' static pressure, but even these are within experimental error. Figure10 illustrates the sensitivity of static pressure to turbulence which has an impact on the selection of reference pressure when making measurements in boundary layer flows. The mean value of static pressure is significantly sensitive to distance from the surface; Tsuji et al. (2007) showed minimum values of static pressure at a height of approximately 10% of the boundary layer thickness, but the results in tables 7 and 8 suggest a much lower height proportionally in the ABL. Komerath et al. (1985) observed that in pipe flow the static pressure fluctuations within the flow exceeded those recorded at the surface, which is consistent with the results here.

4. COMPARISON WITH LABORATORY FLOWS

Wind-tunnel work by Tsuji et al. (2007) is the only work known to the authors that measures the static pressure at the surface and within a turbulent boundary layer. The static pressure within the flow was sensed by a small static probe aligned to the mean flow direction. Their observations were made over a Reynolds Number based on momentum thickness of the boundary layer (θ) of 5000 to 20000, in a boundary layer of thickness (δ) 52 to 62 mm (*Re* dependent). The equivalent value for the ABL is $R_\theta \sim 10^7$. For the logarithmic region of the boundary layer, they (Tsuji et al 2007, figure 9 'log region') found that the static pressure spectrum had a power-law decay between -1.2 and -1.5, which encompasses the present ABL measurements. Tsuji's measurements also included mean static pressure, and showed that the pressure at the surface is below the free-stream static pressure. Also there is a significant decrease in pressure in the lower part of the boundary layer, represented by a minimum pressure coefficient of -0.006 based on free-stream dynamic pressure. Whilst there is no direct comparison with the ABL measurements described here, an estimate from the results in table 8 for z = 6 m gives a pressure coefficient of approximately -0.14 (based on the estimated dynamic pressure at δ), although the minimum may be well above the height at which measurements were made. The root-mean-square values of static pressure have a maximum value of a little over 1% of free-stream dynamic pressure in the study by Tsuji et al. (2007), compared to an estimate of around 3 to 7% or more in the ABL.

Goody (2004) reports surface pressure measurements beneath a two-dimensional, zero-pressure-gradient boundary layer made by seven research groups. The empirical spectral model of these surface pressure fluctuations developed by Goody is compared with the full-scale ABL measurements made in 2000 in figure 11, where the Reynolds number, *Re*, used in the comparison is based on the frictional velocity at the ground (u_τ) and the boundary-layer thickness (δ). The comparison is presented graphically using the scaling defined by Goody. Although there is a considerable difference in Reynolds number, the ABL measurements at an estimated $R_\delta \sim 10^8$ are consistent with the indications from wind-tunnel measurements where $R_\delta \sim 10^5$. Only an order of magnitude can be estimated as the ABL boundary-layer thickness is not known, but as there is no overlap of measurements with the timescale it is only the gradients of the lines that are comparable.

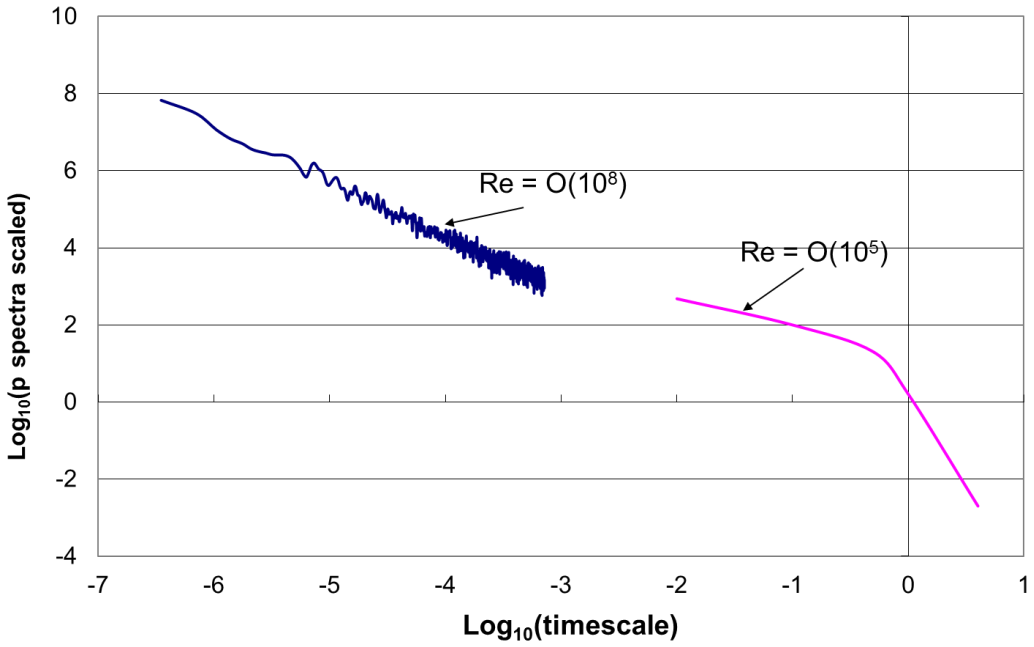

FIGURE 11 Pressure spectra scaled by inner variables (see Goody 2004)

The measurements by Komerath et al. (1985) for pipe flow, show that the spectrum of static pressure decays at a slower rate than does dynamic pressure, but the presentation is not in a form to assess the decay rate.

There is evidence (Lim et al. 2007) of Reynolds-number sensitivity in the magnitude of the core pressure in regions of stable vortex flows around bluff bodies. This implies that in a simulated ABL flow and low *Re* boundary-layer flows in a wind tunnel, the core pressure within vortex type structures will underestimate that of a high *Re* flow: an observation that is consistent with the results from Tsuji et al. (2007) and Goody (2004).

5. COMPARISON WITH OTHER FULL-SCALE MEASUREMENTS

In 1998, Albertson et al. published a paper on measurements of static pressure in the flow over a grass-covered forest clearing. The introduction to the paper states: 'Turbulent fluctuating static pressure is perhaps the least understood basic flow variable in the atmospheric surface layer (ASL)', and the paper continues to elaborate on the difficulty of measuring this variable. Albertson et al. used a fundamentally different sensor from the probes used here, consisting of two horizontal flat plates, 150 mm in diameter, 100 mm apart with a central 2 mm tap on the inside of each plate (Robertson 1972).

Two figures from Albertson et al. (1998) are reproduced in figures 12 and 13 which show two of their representative runs. Velocity was measured at a height of 1.55 m above ground using a sonic anemometer (Gill Instruments) of the same type as used in the Silsoe experiments. Figure 12 shows the longitudinal-velocity power spectra with the $n^{-5/3}$ line for comparison: this is similar to figures 4 and 6 and is consistent with the observation in tables 3 and 5. The corresponding measurements of pressure 0.3 m to one side of the sonic anemometer are reproduced in figure 13. Albertson et al. (1998) show two lines, the $n^{-7/3}$ after Kolmogorov (1941), and $n^{-3/2}$ suggested by Elliott (1972). An additional line for $n^{-4/3}$ has been added by the authors, and as with figures 4 and 6, it is in close agreement with the observed spectra. Albertson did not propose a -4/3 decay and expressed a view on alternative reasons for the observation. In personal contact with Albertson, who is no longer active in this area of research, he was unable to comment further on the observations, but it should be recognized that his measurements were the first published work that observed the near -4/3 decay.

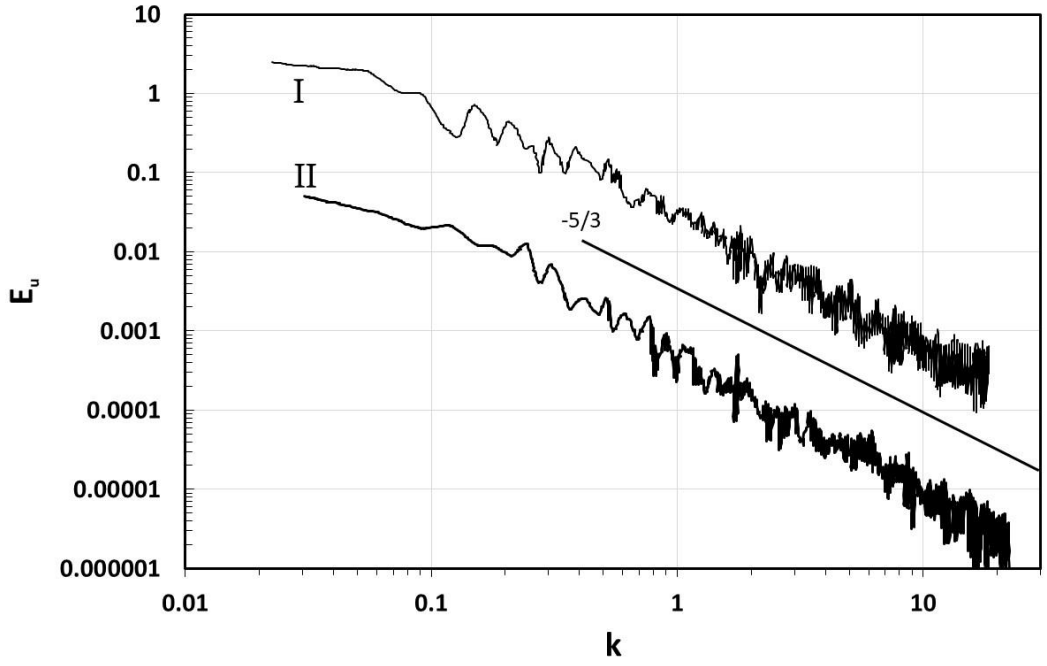

FIGURE 12. Longitudinal-velocity power spectra E_u for two sample files from Albertson et al. (1998) FIG 1.(a), where k is the wave number ($2\pi n/U$).

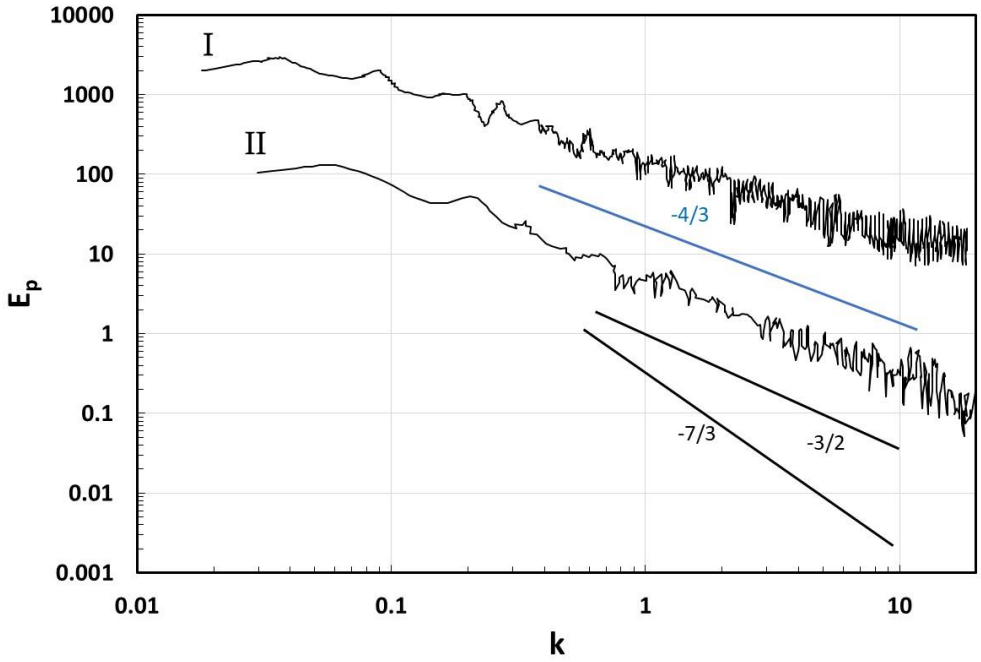

FIGURE 13. Power spectra of static pressure E_p for two sample files by Albertson et al. (1998) FIG 4 (a), with -4/3 line added

6. A VORTEX MODEL

Attempts by dimensional or alternative analyses to corroborate the observed spectral property of static pressure have so far proved unfruitful. Numerical experiments with a vortex model, described in Appendix B, have, however, been helpful in understanding the processes in turbulent shear flows. The model represents Eulerian flow at a single sensing point in turbulent shear flow composed of discrete eddies, but not necessarily a boundary layer flow.

The indications from the very simplified model presented here are that spectral properties of some parameters are well represented by a very limited number of vortices, but some statistical properties are sensitive to further refinement of the model to include additional vortices to enhance turbulence levels. The model includes the inclination of the vortices to produce a shear flow, but the transverse velocity component which is sensitive to yaw of the vortex has not been included. The indications from the model are that when the spectral decay rate of wind dynamic pressure agrees with the experimental findings of -5/3, then the spectral decay rate of static pressure consistently has an exponent close to -4/3. The value of -7/3 that appears in the literature is thus not supported by the simple model.

508 The main reason for exploring a model of this type is to assist in the identification of vortical
509 structures in the ABL. Single-point Eulerian measurement of velocity is clearly insufficient as the
510 model shows that there is no unique velocity 'signature' of a vortex as it depends on the path of
511 the core of the vortex. Measurement of static pressure adds significant information, in relation to
512 vortex size, magnitude and presence, but not to location, pitch angle or yaw angle. In combination
513 with the velocity measurements, further information can be deduced, although not to an extent that
514 enables a mechanistic solution to be developed since it has not been possible in the experiments to
515 measure static pressure at exactly the same position as velocity.
516
517 **7. CONCLUSIONS**
518 The two sets of field measurements provide strong and consistent evidence that in the inertial
519 subrange the spectral pattern of static pressure in the lower part of the ABL has a decay rate close
520 to an exponent of -4/3 (±2.5% or better for each of 4 measurements at 4 different heights). In such
521 a flow, the wind speed and the wind dynamic pressure conform to a decay rate with the expected
522 exponent of -5/3 (±6% or better for each of 4 measurements at 4 different heights). These decay
523 rates accord with those found in the full-scale study by Albertson et al. (1998). Measurements
524 made in a wind tunnel (Tsuji et al. 2007 and Goody 2004) indicate a similar finding although a
525 Reynolds-number sensitivity introduces higher decay rates at low *Re*. Albertson et al are the only
526 comparative measurements that show the coincident velocity spectrum and this had a -5/3 decay.
527 The mean static pressure within the boundary layer compared to 'true static' pressure,
528 defined as the static pressure in the low turbulent freestream flow above a boundary layer, has been
529 calculated. It has been shown that the mean of the second moment of static pressure about 'true
530 static' is equal to the variance of local dynamic pressure. This relationship enables an estimate of
531 the local static pressure in comparison with 'true static' pressure to be made when p_{RMS} and q_{RMS}
532 are known. The significance of this result is that measurements made with a reference pressure
533 from above the boundary layer in a wind tunnel flow will not equate with a reference pressure
534 from a tapping in the surface, and not with full-scale comparison where reference pressure is
535 dependent on location and turbulence level.
536 A simple vortex model of Eulerian flow has been developed which was designed to give an
537 $n^{-5/3}$ decay for wind dynamic pressure spectra; this model then yields an $n^{-4/3}$ decay for the static
538 pressure spectra. The model does show that the static pressure spectral decay is dependent on the

velocity spectral decay and that the -4/3 value will only apply in the inertial subrange where the velocity (or dynamic pressure) spectrum has a decay of $n^{-5/3}$. The cospectrum of Reynolds stress is also well represented in the vortex model. The model has the potential to be developed further to produce more realistic levels of turbulence, but was adequate for the spectral pattern described here.

ACKNOWLEDGEMENTS

Figures 12 & 13 have been reproduced from Albertson, JD, Kata, GG, Pariange, MB, Eichinger, WE. Spectral scaling of static pressure fluctuations in the atmospheric surface layer: The interaction between large and small scales. Physics of Fluids, Vol **10,** No 7, July 1998 with the permission of AIP Publishing. The measurements in 2000 were part of the science programme conducted at Silsoe Research Institute, and funded by the BBSRC. The measurements in 2015/16 followed full-scale measurements made on the Silsoe site as part of the EPSRC funded Refresh Programme (Ref EP/K031893/1), and formed part of the contribution to the Programme by the University of Birmingham.

DATA AVAILABILITY STATEMENT

The data that support the findings of this study are available from the corresponding author (roger@hoxey.com) and also from Andrew Quinn (a.d.quinn@bham.ac.uk), Peter Richards (pj.richards@auckland.ac.nz) and Adam Robertson (adamprobertson@gmail.com) upon reasonable request.

APPENDIX A.

A1. A Probe for Measuring Static Pressure in the ABL

A traditional static probe of the type often incorporated into a pitot-static probe is not designed for use in turbulent flow which has significant variations in yaw and pitch (Bryer & Pankhurst, 1971). An early meteorological instrument developed by Dines (Meteorological Office, 1956) incorporated a directional pitot tube for total pressure and a vertical tube with tapping holes around its circumference, making the instrument insensitive to the horizontal flow direction. The device was used for many years as the standard instrument for measuring wind speed in many countries including Australia where its performance has recently been assessed by Miller et al. (2013). The instrument was found to have a pressure coefficient of approximately 1.5 (*Re* dependent), comprising 1.0 for the pitot and -0.5 for the integrated pressure around the vertical tube.

The vertical tube with circumferential tapping holes was developed by Marshall (1976) as a stand-alone instrument by adding a shroud around the tapping holes which could be adjusted to give zero pressure coefficient. A smaller version of this probe (figure 15) was developed at Silsoe Research Institute for full-scale measurements with the addition of a collar which is easily adjusted for probe calibration. Details of the probe and its calibration are given in Moran & Hoxey (1979) with key results summarized here.

The static probe was initially calibrated on a cut grass field in natural wind with a mean wind speed of 7 m s^{-1}. It was mounted 3 m above ground and the sensed pressure compared to the pressure from a ground surface tapping. The collar was adjusted to give mean zero pressure difference. The probe was then mounted in a low turbulence wind tunnel where it was found to have a pressure coefficient of +0.07. Initially all other probes were calibrated in the wind tunnel to give the same pressure coefficient. The probe was checked for sensitivity to pitch and Reynolds number in the wind tunnel: for $\pm 5^{o}$ of pitch the probe had a +1% error and over the range of wind speeds in the full-scale experiment the variation with increasing wind speed was -2%. In combination these errors partially cancel each other giving an overall estimate of error of ±1½% of wind dynamic pressure.

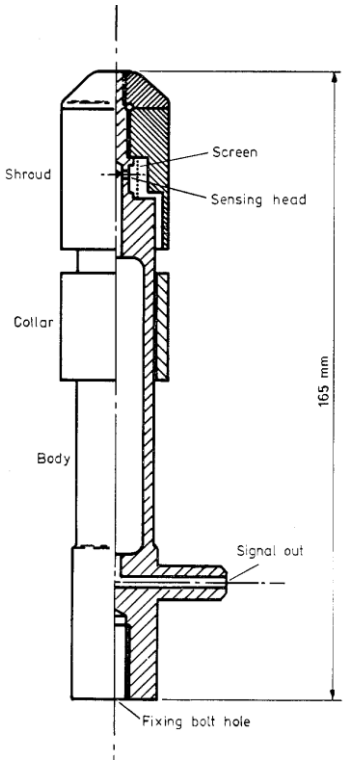

FIGURE 15. Part cut-away drawing of the static probe, the shroud and collar had a diameter of 28 mm.

The difference between the full-scale and wind-tunnel calibration was not explained until more recently when preliminary experiments of the type described here showed that the mean static pressure in the ABL initially decreases with height from the ground. By setting the pressure difference from the probe at 3 m to the ground tap to 'zero' is incorrect: the wind-tunnel calibration now indicates that there is a mean pressure coefficient difference of -0.07 between 3 m above ground and the ground level tapping in the field experiment.

For the probes used in the experiments described here, the wind-tunnel calibration procedure was changed and the collar was set to give zero pressure coefficient in low-turbulence flow.

APPENDIX B.

B1. A Simple Vortex Model

A simple Rankine-type vortex model has been developed of the Eulerian flow past a single point in a shear flow to represent the full-scale measurements that have been made. The vortex model with circulation Γ, in a continuous mathematical form, has been used, consisting of a rotational core (radius a) and an irrotational outer region. The tangential velocity (V) at a radius r is

$$V(r) = \Gamma . r/(a^2 + r^2)$$

The vortex is assumed to move in a stream of constant velocity, U; hence the fluctuating velocity components (u' and v'), as sensed at a fixed point distance d from the line of passage of the vortex are

$$u'(t) = \frac{\Gamma d}{(Ut)^2 + d^2 + a^2}$$

$$v'(t) = \frac{\Gamma U t}{(Ut)^2 + d^2 + a^2}$$

The corresponding static pressure (p') is

$$p'(t) = -\frac{1}{2}\rho \frac{\Gamma^2}{(Ut)^2 + d^2 + a^2}$$

The energy spectra of wind dynamic pressure (*Eq(n)*) and of static pressure (*Ep(n)*) for a single vortex have been calculated using a standard FFT algorithm with 4096 points and are shown in figure 16, where the spectra have been divided by the integrated spectrum of the wind dynamic pressure; a procedure that has been adopted throughout this paper. The vortex has been inclined to the vertical to represent shear in the simulated flow, giving a time-dependent vertical velocity (w'). The dynamic pressure has been calculated from the velocity components, from which the Reynolds stress ($-\rho u'w'$) has also been derived. The parameters used in the single-vortex model are: circulation Γ ($m^2 s^{-1}$) = 100, core diameter a (m) = 20, distance d (m) = 40, inclination (degrees) = 25 in a stream U ($m s^{-1}$) = 8.

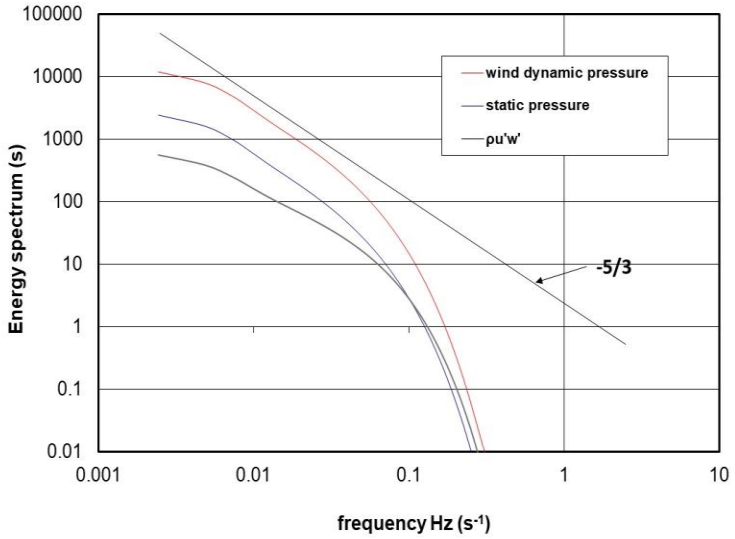

FIGURE 16. Energy spectra of a single vortex model.

The spectral pattern by adding a second smaller vortex (circulation Γ ($m^2 s^{-1}$) = 10, core diameter *a* (m) = 2, distance *d* (m) = -4, inclination (degrees) = 25) is shown in figure 17, and adds higher frequency energy. The spectra for wind dynamic pressure and static pressure are similar in these examples, as the distance of the observer from the vortex core (*d*) is greater than the rotational core radius (*a*). . Examination of *Eq(n)* and *Ep(n)* shows that when the vortex core passes close to the observer, *Eq(n)* is smaller than *Ep(n)*. This is a significant result as it explains why, in a complex passage of vortices, the spectral pattern of static pressure will decay at a slower rate.

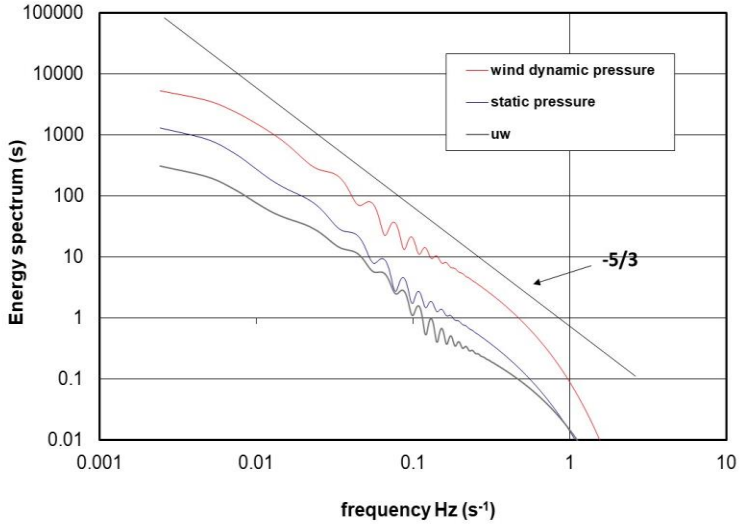

FIGURE 17. Energy spectra of a two vortex model.

A small number of additional vortices of different intensity, core size and path distance from the stationary observer, randomly occurring in the time series, were added to the single-vortex model. Within the concept of a simple vortex model, shear is introduced by inclining the vortex from the vertical. To attain the desired shear for a boundary-layer, vortices are required to be inclined forward by 20°-30° from the vertical. A multiple vortex model was constructed consisting of only 4 pairs of vortices, one of each pair passing each side of the observer. The quantities used in the model are given in table 9, where the stream speed U was 8 ms^{-1}.

Circulation Γ ($m^2 s^{-1}$)	100	10	2	0.1
Core diameter a (m)	20	2	0.2	0.02
Distance d (m)	±40	±4	±0.4	±0.01
Inclination (degrees)	25	25	25	25

TABLE 9. Quantities used in the vortex model.

Continuing to add smaller vortices adds energy to the spectrum at higher frequency and it was found that 8 vortices were sufficient to give an energy spectrum close to the spectrum of dynamic pressure and of static pressure measured at a height of 6 m in the full-scale measurements. This is shown in figure 18; the same windowing was applied to the spectra for presentation smoothing as was applied to all full-scale measurements to maintain consistency.

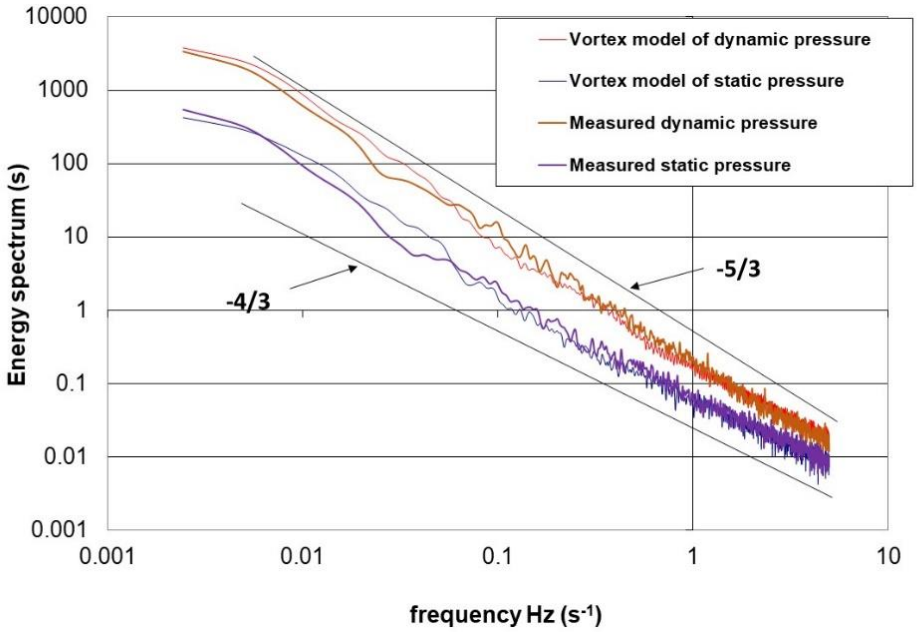

FIGURE 18. Wind dynamic pressure and static pressure spectra of a multiple vortex model compared to the measured spectra.

The selection of vortices influences the spectral decay rate and hence the target for the dynamic pressure spectrum was set to $n^{-5/3}$. This is the case in figure 18, and the coincident static pressure spectrum, also shown in figure 18, has a decay close to $n^{-4/3}$. The cospectral density of the streamwise and vertical components, i.e. the Reynolds-stress cospectrum, is shown in figure 19. The selection of only 4 pairs of vortices appears adequate for the representation of wind dynamic pressure and static pressure but not sufficient for the Reynolds-stress cospectrum, although the model provides an indication of the experimental observed finding. The model is possibly inadequate as all the vortices were inclined at 25 degrees; this gave $u_\tau/U = 0.033$, half of the measured value. More vortices are needed and the inclination angle randomized with a suitable bias; the indication from figure 19 is of a lower inclination angle for large vortices. The 8-vortex model produced a turbulence intensity of 5%, which is only a quarter of the measured level and hence is not a representation of the flow statistics.

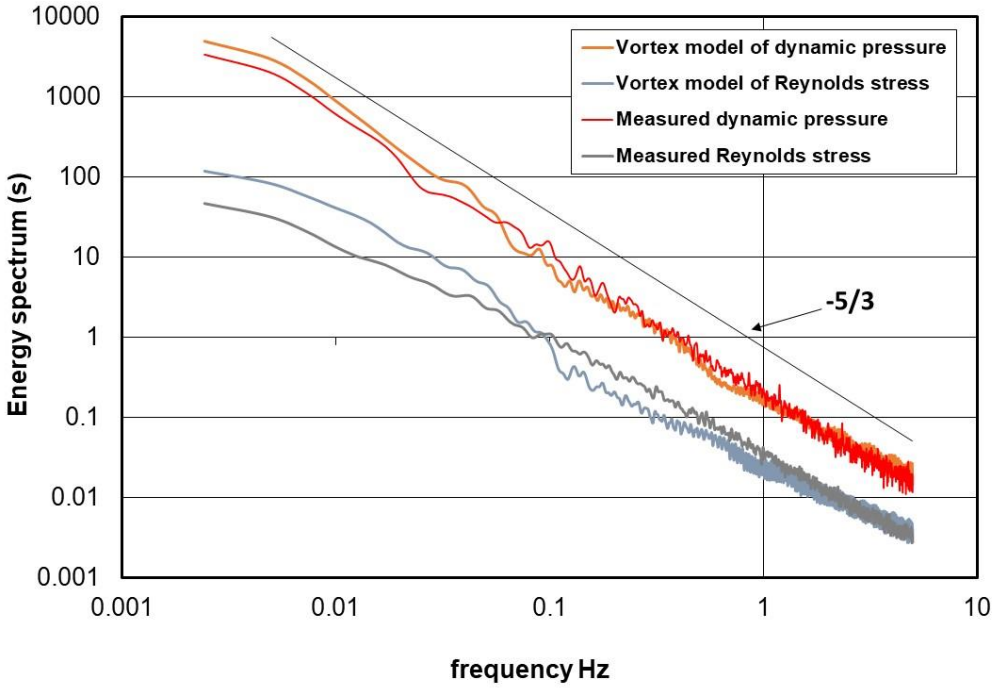

FIGURE 19. Reynolds-stress cospectral properties of a multiple vortex model

B2. Concluding comments

The properties of the simple vortex model proposed of shear flow contain many of the spectral characteristics found in experimentally-measured, near-surface boundary-layer wind. Specifically:

(i) spectral decay for the velocity components and of the wind dynamic pressure approximating to $n^{-5/3}$

(ii) static pressure spectrum with a decay rate approximating to $n^{-4/3}$

(iii) Reynolds-stress cospectrum with a decay similar to experiment.

The simple vortex model does not represent a turbulent boundary layer but only the Eulerian flow past a stationary measurement point in a shear flow. Although the 8-vortex model produced a turbulence intensity of only 5%, a quarter of the measured level, the model correctly represents the measured spectra for dynamic pressure and, importantly, provides corroboration on the near $n^{-4/3}$ decay in the static pressure spectrum that was observed experimentally in the full-scale measurements. The model suggests that the flow can be represented by a cascade of discrete vortices and would be useful in computational analyses.

REFERENCES

Albertson JD, Katual GG, Pariange MB, Eichinger WE (1998) Spectral scaling of static pressure fluctuations in the atmospheric surface layer: The interaction between large and small scales. Physics of Fluids, Vol **10,** No 7, July 1998

Bryer DW, Pankherst RC (1971) Pressure-probe methods for determining wind speed and flow direction. National Physical Laboratory, HMSO, London, UK, pp 125

Elliott JA (1972) Microscale pressure fluctuations measured within the lower atmospheric boundary layer. J. Fluid Mech **53**, 351 (1972)

Goody M (2004) Empirical spectral model of surface pressure fluctuations. AIAA Journal, Vol. **42**, No. 9, 1788 – 1794, September 2004

Gough, H., Sato, T., Halios, C., Grimmond, C.S.B., Luo, Z., Barlow, J.F., Robertson, A., Hoxey, A., Quinn, A., 2018 Effects of variability of local winds on cross ventilation for a simplified building within a full-scale asymmetric array: The Silsoe field campaign (in review). J. Wind Eng. Ind. Aerodyn. Vol **175**, 408-418.

Hoxey RP, Richards PJ (1992) Structure of the atmospheric boundary layer below 25 m and implications to wind loading on low-rise buildings. J.Wind Eng. Ind. Aerodyn. **41-44,** 317-327.

Hoxey RP, Richards PJ (1995) Full-scale wind load measurements point the way forward. J.Wind Eng. Ind. Aerodyn. **57,** 215-214.

Hoxey RP, Reynolds AM, Richardson GM, Robertson AP, Short JL (1998) Observation of Reynolds number sensitivity in the separated flow region on a bluff body. J.Wind Eng. Ind. Aerodyn. **73,** 231-249

Hunt, JCR, Morrison, JF (2000). Eddy Structures in Turbulent Boundary Layers. Euro J. Mech. B – Fluids **19**, 673-694

Hutchins N, Chauhan K, Marusic I, Monty J, Klewicki J (2012) Towards Reconciling the Large-Scale Structure of Turbulent Boundary Layers in the Atmosphere and Laboratory. Boundary-Layer Meteorol., Vol **145**, 273-306.

Kolmogorov AN (1941) The local structure of turbulence in incompressible viscous fluid at very large Reynolds numbers. Dik1. Akad. Nauk SSSR 30 [reprinted in Proc. R. Soc., London Ser. A, 434, 9 (1941)]

Komerath NM, Hegde UG, Strahle WC (1985) Turbulent Static Pressure Fluctuations away from Flow Boundaries. AIAA Journal, Vol **23**, No 9, 1320-1326

Lim HC, Castro IP, Hoxey RP (2007) Bluff bodies in deep turbulent boundary layers: Reynolds-number issues. J. Fluid Mech, **571**, 97-118

Marshall, R D (1976) Ambient Pressure Probe, US Patent Application, 3950995A

Meteorological Office (1956) Handbook of Meteorological Instruments. Part I—Instruments forSurface Observations, H. M. Stationary Office, UK, 468 pp

Miller C, Holmes J, Henderson D, Ginger J, and Morrison M. (2013) The Response of the Dines Anemometer to Gusts and Comparisons with Cup Anemometers, Journal of Atmospheric and Oceanic Technology, Vol **30**, 1320-1336

Miles Nl,, Wangaard JC (2004) Turbulent Pressure Statistics in the Atmospheric Boundary Layer from Large-Eddy Simulation, Boundary Layer Meteorology, **113,** 161-185.

Moran P, Hoxey RP (1979) A probe for sensing static pressure in two-dimensional flow. J. Phys. E: Sci. Instrum., **12**, pp752-3

Morrison JF, Subramanian CS, Bradshaw P (1992) Bursts and the law of the wall in turbulent boundary layers. J. Fluid Mech., **241**, 75-108

Nishiyama RT, Bedard AJ (1991) A quad-disc static pressure probe for measurements in adverse atmospheres: With a comparative review of static pressure probe designs. Review of Scientific Instruments, 62, 2193-2204.

743 Otnes RK, Enochson L (1972) Digital Time Series Analysis. A Wiley – Interscience Publication, pp 467

744 Robertson P (1972) A direction-insensitive static head sensor. J. Phys. E: Sci. Instrum., **5**, 1080

745 Richards PJ, Fong S, Hoxey RP (1997)) Anisotropic turbulence in the atmospheric surface layer, J. Wind Eng.
746 Ind. Aerodyn. **69-71**, 903-913

747 Richards PJ, Hoxey RP, Short JL. (2000) Spectral models for the neutral atmospheric surface layer, J. Wind Eng.
748 Ind. Aerodyn. **87**, 167-185

749 Richards PJ, Hoxey RP, Short JL (2001) Wind pressures on a 6 m Cube, J. Wind Eng. Ind. Aerodyn., **89** (14-
750 15), 1553-1560

751 Tsuji Y, Fransson JHM, Alfredsson PH, Johansson AV (2007) Pressure statistics and their scaling in high-
752 Reynolds-number turbulent boundary layers. J.Fluid Mech. (2007), **585**, 1-40
753